Scaling Laws for Optimal Power-Law Fluid Flow within Converging-Diverging Dendritic Networks of Tubes and Rectangular Channels

Ashish Garg[1,2*]

[1]Seminare Private Limited, Delhi, India

[2]Department of Chemical Engineering, Indian Institute of Technology Delhi, India

Abstract

Power-law fluid flows in the converging-diverging tubes and rectangular channel are prevalent in engineered microfluidic devices, many industrial processes and heat transfer applications. We analyzed optimal flow conditions and network structures for power-law fluids in linear, parabolic, hyperbolic, hyperbolic cosine and sinusoidal converging-diverging dendritic networks of tubes and rectangular channels, and aiming to maximize flow conductance under volume and surface-area constraints. This model shed light on strategies to achieve efficient fluid transport within these complex dendritic networks. Our study focused on steady, incompressible, 2D planar and axisymmetric laminar flow without considering network losses. We found that the flow conductance is highly sensitive to network geometry. The maximum conductance occurs when a specific radius/channel-height ratio β is achieved. This value depends on the constraint as well as on the vessel geometry such as tube or rectangular channel. However independent of the kind of the converging-diverging profile along the length of the vessel. We found that the scaling, i.e., $\beta^*_{\max} = \beta^*_{\min} = N^{-1/3}$ for constrained tube volume and $\beta^*_{\max} = \beta^*_{\min} = N^{-(n+1)/(3n+2)}$ for constrained surface area for all converging-diverging tube-networks profile remains the same as found by Garg et al. [1] for the power-law fluid flow in a uniform tube. Here, $\beta^*_{\max}$, $\beta^*_{\min}$ are the radius ratios of daughter-parent pair at the maximum divergent part or minimum convergent part of the vessel. N represents the number of branches splitting at each junction, and n is the power-law index of the fluid. Further, we found that the optimal flow scaling for the height ratio in the rectangular channel, i.e., $\beta^*_{\max} = \beta^*_{\min} = N^{-1/2}\alpha^{-1/2}$ for constrained tube volume and $\beta^*_{\max} = \beta^*_{\min} = N^{-1/2}\alpha^{-n/(2n+2)}$ for constrained surface area for all converging-diverging channel-networks, respectively, where α is the channel-width ratio between parent and daughter branches. We validated our results with experiments, existing theory for limiting conditions, and extended Hess-Murray's law to encompass shear-thinning and shear-thickening fluids for any branching number N.

Keywords: Tree-like networks, Converging-Diverging dendritic networks, Self-similar networks, Flow in tubes and rectangular channels, flow resistance, flow conductance, Constrained network surface area, Constrained network volume, Power-law fluids, Optimal flow conditions, Hess–Murray law, Constructal law.

*Email: **ashish.garg.iisc@gmail.com, ashish@seminare.in** May 8, 2024

1 Introduction

Fluid flow through intricate tree-like dendritic networks is ubiquitous in nature, from blood vessels in our bodies to the branching structures of plants as well as in the technology [2–5, 5–7]. The understanding and optimizing this flow is crucial in various fields, including microfluidics, biomedical engineering, and even designing efficient transport systems. These networks resemble branching structures like trees, with a self-similar repeating pattern. This work investigate the fractal dendritic networks. However, unlike typical fluid systems with simple cylindrical tubes, these networks can have a combination of converging-diverging or corrugated tubes and rectangular channels. Our focus is on power-law fluids. These fluids exhibit a non-linear relationship between shear stress and shear rate, making their flow behavior more complex compared to Newtonian fluids (like water) [8, 9].

Understanding how non-Newtonian fluids, like power-law fluids, behave in converging-diverging corrugated channels is vital for many industrial processes. These complex fluid properties combined with the structured geometry of corrugated channels benefit various applications. In flexographic printing, they control ink thickness [10, 11]; in food processing, they ensure uniform coating [12, 13]; in polymer processing, corrugated channels are used in extrusion and injection molding processes where they optimize flow [14, 15]; in oil and gas, they enhance transportation efficiency [16]. They are also crucial in biomedical drug delivery systems [17] and wastewater treatment [18–21]. The recirculation formed in corrugation valleys enhances heat transfer [22], offering valuable insights into fluid dynamics and heat transfer properties, essential for industrial system optimization. Additionally, in the fabrication of impact-absorbing fabric materials, shear-thickening fluids, a combination of Newtonian, power-law shear thinning, and shear thickening fluids depending on the applied shear rate, flow through such converging-diverging porous geometries [23, 24]. A schematic of a dendritic tree-like converging-diverging tube or rectangular channel network is depicted in Figure 1. This network has a bifurcation number of $N = 2$ and extends up to $k = 4$ generations of branches. Here $R_{\max}$, $R_{\min}$ and $H_{\max}$, $H_{\min}$ are the maximum and minimum radius or height of the tube and channel, respectively.

Scaling laws provide powerful relationships between different network parameters, allowing us to predict flow behavior across different network sizes. Expanding upon Murray's application of the principle of minimum work in circular tubes [25], researchers have investigated flow dynamics in tree-like branching networks. For instance, Revellin et al. [26] extended Murray's law to analyze non-Newtonian power-law fluid flow in two channels, revealing a constant diameter ratio ($D_{(k+1)}/D_k = 2^{-1/3}$) for the optimal flow irrespective of the fluid's power-law index n. Advancements by Garg et al. [1, 27, 28] delved into networks with varying branching numbers and power-law indices, examining circular and elliptical cross-sections under volume and surface area constraints for both laminar and turbulent flows. Notably, in the laminar flow regime, Garg et al. [1, 27] discovered that under volume constraints, the optimal radius/diameter/length relationship remains consistent regardless of the fluid's shear-thinning or shear-thickening behavior, denoted as $(D_{(k+1)}/D_k)^* = N^{-1/3}$. However, under surface area constraints, this relationship becomes significantly influenced by the power-law index, expressed as $(D_{(k+1)}/D_k)^* = N^{-(n+1)/(3n+2)}$. For turbulent flow, Garg et al. [28] identified scaling pat-

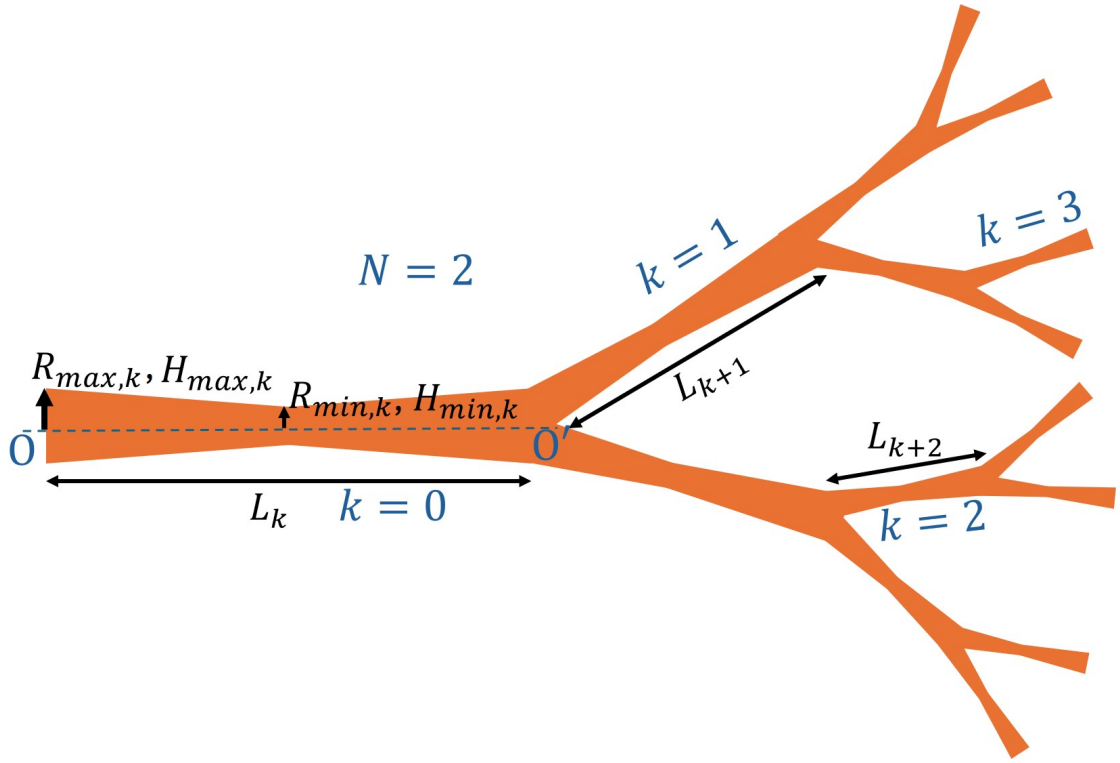

Figure 1: This schematic depicts a self-similar dendritic structure. Here $R_{\max}$, $R_{\min}$ and $H_{\max}$, $H_{\min}$ are the maximum and minimum radius or height of the tube and channel, respectively. The k represents the generation level. N, the bifurcation number of branches splitting. L denotes the tube/channel length.

terns for smooth and rough tube networks, respectively described as $\frac{D_{k+1}}{D_k} = \beta^* = N^{-(10n+1)/(24n+3)}$ and $\frac{D_{k+1}}{D_k} = N^{-3/7}$, respectively. In a recent study Garg [29], investigate the yield stress fluid flow in tree-like networks where proposing the conjecture with its proof, they find that one of the optimal solution obey Murray law under constraint volume. Additionally, Lee et al. [30] introduced a theory on capillary microchannel flows within tree-like branches, while investigations at the nanoscale, conducted by Garg [21, 31], Garg and Bishnoi [32] and Mishra and Garg [33], explored the impact of network geometry on Newtonian fluid behavior, adding further complexity to the analysis.

Prior research on converging-diverging tubes and rectangular channels tree-like networks has established various flow scaling relationships, however these studies are quite limited and had different focus. Jing and Zhan [34] studied the electro-osmotic Flow in fractal converging diverging width of the rectangular network, where they find the optimal width ratio is proportional to branching number as $1/N$. Further [35] studied an analytical model for the effective permeability of fractal branched networks composed of converging–diverging capillaries. This study aims to unveil the scaling laws governing the optimal flow of power-law fluids within these intricate converging-diverging or corrugated tubes and rectangular channels dendritic networks. By analyzing the interplay between power-law behavior, converging-diverging geometries, and the network's fractal nature, we aim to develop an analytical model for optimizing flow within these systems. In this study, we investigate the linear,

parabolic, hyperbolic, hyperbolic cosine and sinusoidal converging-diverging tubes and rectangular channel and provide scaling laws for all in a generalised framework. This model will shed light on strategies to achieve efficient fluid transport within these complex dendritic networks. The paper is structured as follows. Section 2 details the axisymmetric model for the tube and the 2D planar model for the rectangular channels under the lubrication approximation in a single converging- diverging vessel. Section 3 explores the concepts of flow resistance and conductance for tree-like self-similar branching networks under volume and surface-area constraints. Section 4 presents the results and discussions. Finally, Section 5 concludes the paper.

2 Theoretical model: Axisymmetric and 2D planar model

We examine the steady, incompressible, without body forces such as the gravitational effect is negligible, 2D planar and axisymmetric laminar flow of an incompressible power-law non-Newtonian fluid within a circular tube and rectangular shallow cross-section of a channel. The tube has a varying radius $R(x)$ along the length L, whereas the channel has a varying height $H(x)$ and a constant width W along the length L, as illustrated in figures 2. These figures depict five distinct converging-diverging geometries: linear in (a); parabolic, hyperbolic, and yperbolic cosine in (b); and the sinusoidal (c) converging-diverging tube and channel. The tube is assumed to be considerably long in comparison to its radius and the channel is considerably long and wide compared to its height, satisfying $R(x)/L \ll 1$, $H(x)/W \ll 1$ and $H(x)/L \ll 1$, allowing for a axisymmetric and two-dimensional planar model under lubrication limits [31].

The mid-plane origin of the tube is the centreline at mid length or between the plates, with the flow domain extending from $x = -L/2$ to $x = L/2$. Let the cartesian velocity components u represent the longitudinal velocity along x direction. Here the r represents the radial direction in tube, and z direction denotes the vertical direction in the channel, respectively. Under lubrication assumptions, the leading-order solution ensures the radial and the normal velocity vanishes everywhere. In addition, the leading order pressure gradient along radial and normal direction also vanishes, i.e.,

$$\frac{\partial p}{\partial r} = 0, \quad \text{in the tube, and} \quad \frac{\partial p}{\partial z} = 0 \quad \text{in the channel,} \tag{1}$$

respectively. Here pressure p is only the function of x at the leading order. Therefore $\dfrac{\partial p}{\partial x} = \dfrac{dp}{dx}$. For an infinitesimal length, dx, of the tube or channel, the infinitesimal pressure drop for a given flow rate Q can be written as

$$dp = \frac{2KQ^n(3n+1)^n dx}{\pi^n n^n R(x)^{(3n+1)}}, \quad \text{for tube, and} \quad dp = \frac{KQ^n(2n+1)^n dx}{2^n W^n n^n H(x)^{(2n+1)}} \quad \text{for channel,} \tag{2}$$

respectively [36, 37]. The above formulation occur for the power-law fluid model as [38]

$$\eta = \frac{\tau}{\dot{\gamma}} = K\dot{\gamma}^{n-1}, \tag{3}$$

(a) Conical tube or rectangular channel

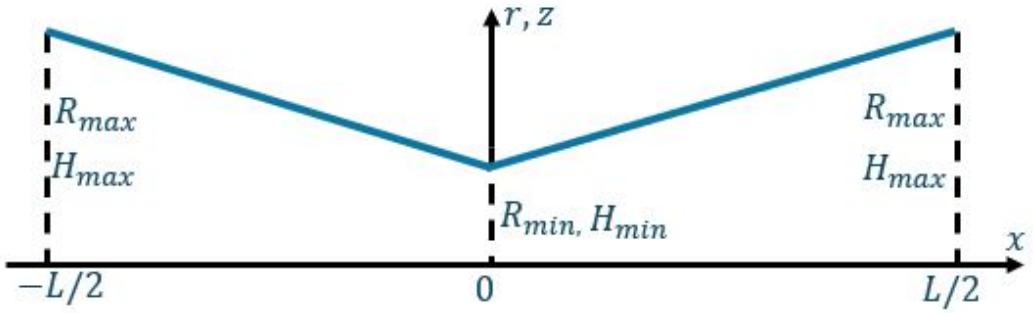

(b) Parabolic, Hyperbolic, Hyperbolic cosine tube or rectangular channel

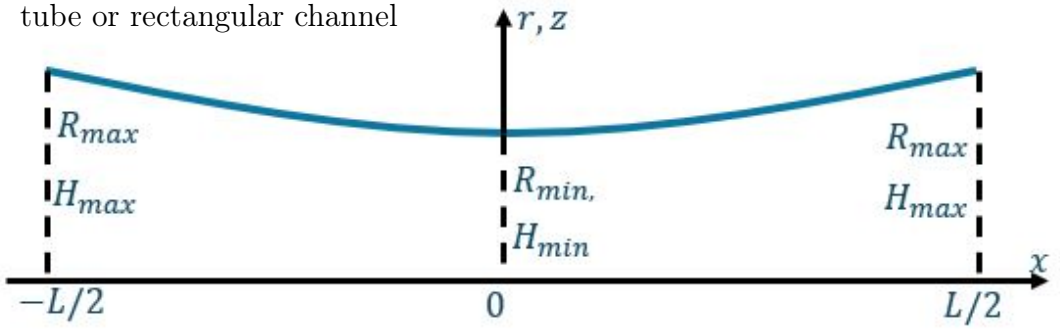

(c) Sinusoidal tube or rectangular channel

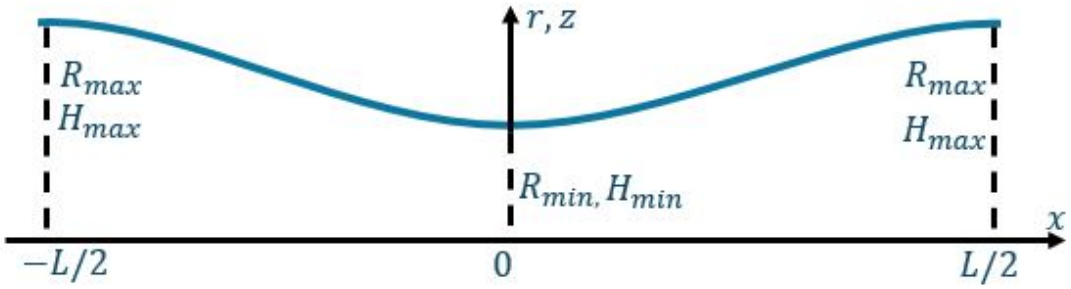

Figure 2: Schematic diagram of the upper half part of the shallow tube or channel of length L. For the tube, the R represents the varying cross–sectional radius across length with $R_{\max}$ and $R_{\min}$ denote the radius at the most divergent and convergent part of the tube. For the channels of constant width W in a branch, the H represents the varying cross–sectional mid-height across length with $H_{\max}$ and $H_{\min}$ denote the channel-height at the most divergent and convergent part of the upper-part/lower-part of the channel. The Cartesian axis is taken at the mid plane of the channel at the throat.

where η is the fluid viscosity, τ is the stress, $\dot{\gamma}$ is the strain rate, K is the consistency factor, and n is the flow behavior index.

In the case of an incompressible fluid, the volumetric flow rate across any arbitrary cross-section of the channel remains the same. Consequently, the total pressure drop across the tube and channel with variable radius $R(x)$ and, height $H(x)$, over a length L is expressed as

$$\Delta P = \frac{2KQ^n(3n+1)^n}{\pi^n n^n}\int_{-L/2}^{L/2}\frac{dx}{R(x)^{(3n+1)}}, \quad \text{for tube, and} \quad \Delta P = \frac{KQ^n(2n+1)^n}{2^n W^n n^n}\int_{-L/2}^{L/2}\frac{dx}{H(x)^{(2n+1)}} \tag{4}$$

for the channel, respectively. Using equation (4), in the following sections, we will derive the analytical

expressions for the relation between pressure drop and volumetric flow rate by using the different definitions of variable radius $R(x)$ and height $H(x)$ profiles for five converging-diverging geometries of axisymmetric tube and 2D planar channels.

2.1 Linear converging-diverging tube and rectangular channel

2.1.1 $\Delta P - Q$ relation for tube

For a corrugated linear converging-diverging tube, as shown in figure 2(a), the radius $R(x)$, varying with the axial coordinate x can be define as

$$R(x) = a + b|x| \quad \text{for} \quad -L/2 \leq x \leq L/2; \quad a > 0,\ b > 0, \tag{5}$$

where

$$a = R_{\min} \quad \text{and} \quad b = \frac{2\left(R_{\max} - R_{\min}\right)}{L}. \tag{6}$$

Using equation (5), the equation (4) leads to

$$\begin{aligned}
\Delta P &= \frac{2KQ^n(3n+1)^n}{\pi^n n^n} \int_{-L/2}^{L/2} \frac{dx}{(a+b|x|)^{3n+1}}, \\
&= \frac{2KQ^n(3n+1)^n}{\pi^n n^n} \left(\left[\frac{1}{3bn(a-bx)^{3n}} \right]_{-L/2}^{0} + \left[-\frac{1}{3bn(a+bx)^{3n}} \right]_{0}^{L/2} \right), \\
&= \frac{4KQ^n(3n+1)^n}{3b\ \pi^n n^{n+1}} \left[\frac{1}{a^{3n}} - \frac{1}{(a+bL/2)^{3n}} \right].
\end{aligned} \tag{7}$$

Further, using the definitions of a, and b from equation (10), we get

$$\Delta P = \frac{2LKQ^n(3n+1)^n}{3\pi^n n^{n+1}\left(R_{\max} - R_{\min}\right)} \left[\frac{1}{R_{\min}^{3n}} - \frac{1}{R_{\max}^{3n}} \right]. \tag{8}$$

Equation (8) is the same as analytical model as derived by Sochi [36].

2.1.2 $\Delta P - Q$ relation for rectangular channel

For a corrugated linear wedge converging-diverging channel, as depicted in figure 2(a), the channel height $H(x)$, varying with the axial coordinate x is expressed as

$$H(x) = a + b|x| \quad \text{for} \quad -L/2 \leq x \leq L/2; \quad a > 0,\ b > 0, \tag{9}$$

where

$$a = H_{\min} \quad \text{and} \quad b = \frac{2\left(H_{\max} - H_{\min}\right)}{L}. \tag{10}$$

Using equation (9), the equation (4) transforms into

$$\begin{aligned}\Delta P &= \frac{KQ^n(2n+1)^n}{2^n W^n n^n}\int_{-L/2}^{L/2}\frac{dx}{(a+b|x|)^{2n+1}},\\ &= \frac{KQ^n(2n+1)^n}{2^n W^n n^n}\left(\left[\frac{1}{2bn(a-bx)^{2n}}\right]_{-L/2}^{0}+\left[-\frac{1}{2bn(a+bx)^{2n}}\right]_{0}^{L/2}\right),\\ &= \frac{2KQ^n(2n+1)^n}{2^{n+1}W^n n^{n+1}b}\left[\frac{1}{a^{2n}}-\frac{1}{(a+bL/2)^{2n}}\right].\end{aligned} \tag{11}$$

Further, using the definitions of a, and b from equation (10), we get

$$\Delta P = \frac{LKQ^n(2n+1)^n}{2^{n+1}W^n n^{n+1}\left(H_{\max}-H_{\min}\right)}\left[\frac{1}{H_{\min}^{2n}}-\frac{1}{H_{\max}^{2n}}\right]. \tag{12}$$

Equation (12) is the same as analytical model as derived by Garg [37] for the converging-diverging rectangular channel. Under the Newtonian and power-law fluid limit, equation (12) is the same as analytical model derived by Vishal et al. [24].

2.2 Other converging-diverging tube and rectangular channel

2.2.1 $\Delta P - Q$ relation for tube

Similarly, for a parabolic, hyperbolic, hyperbolic cosine and sinusoidal converging-diverging tube, (see figure 2(b-c)), $\Delta P - Q$ relations are given by [36]

$$\Delta P = \frac{2LKQ^n(3n+1)^n}{\pi^n n^n R_{\min}^{3n+1}}\left[{}_2F_1\left(\frac{1}{2},3n+1;\frac{3}{2};1-\frac{R_{\max}}{R_{\min}}\right)\right] \quad \text{for parabolic,} \tag{13}$$

$$\Delta P = \frac{2LKQ^n(3n+1)^n}{\pi^n n^n R_{\min}^{3n+1}}\left[{}_2F_1\left(\frac{1}{2},\frac{3n+1}{2};\frac{3}{2};1-\frac{R_{\max}^2}{R_{\min}^2}\right)\right] \quad \text{for hyperbolic,} \tag{14}$$

$$\Delta P = \frac{2KLQ^n(3n+1)^n}{3\pi^n n^{n+1}R_{\min}R_{\max}^{3n}\operatorname{arccosh}\left(\frac{R_{\max}}{R_{\min}}\right)}\operatorname{Im}\left[{}_2F_1\left(\frac{1}{2},\frac{-3n}{2};\frac{2-3n}{2};\frac{R_{\max}^2}{R_{\min}^2}\right)\right], \quad \text{for hyperbolic cosine} \tag{15}$$

and

$$\Delta P = \frac{2KLQ^n(3n+1)^n}{3\pi^{n+1}n^{n+1}R_{\max}^{3n}\sqrt{R_{\max}R_{\min}}}\operatorname{Im}\left(F_1\left(-3n;\frac{1}{2},\frac{1}{2};1-3n;1,\frac{R_{\max}}{R_{\min}}\right)\right), \quad \text{for the sinusoidal,} \tag{16}$$

converging-diverging tubes respectively, where ${}_2F_1$ is the hypergeometric function, $\operatorname{Im}({}_2F_1)$ is the imaginary part of the hypergeometric function and F_1 is the imaginary part of the Appell hypergeometric function in equations (13)-(16). It is worth mentioning that all these relationships maintain dimensional consistency and validated for a Newtonian fluid flow [36].

2.2.2 $\Delta P - Q$ relation for rectangular channel

Similarly, for a parabolic, hyperbolic, hyperbolic cosine and sinusoidal converging-diverging rectangular channel, (see figure 2(b-c)), $\Delta P - Q$ relations are given by [37]

$$\Delta P = \frac{LKQ^n(2n+1)^n}{2^n W^n n^n H_{\min}^{2n+1}} \left[{}_2F_1\left(\frac{1}{2}, 2n+1; \frac{3}{2}; 1 - \frac{H_{\max}}{H_{\min}}\right)\right] \quad \text{for parabolic,} \tag{17}$$

$$\Delta P = \frac{LKQ^n(2n+1)^n}{2^n W^n n^n H_{\min}^{2n+1}} \left[{}_2F_1\left(\frac{1}{2}, \frac{2n+1}{2}; \frac{3}{2}; 1 - \frac{H_{\max}^2}{H_{\min}^2}\right)\right] \quad \text{for hyperbolic,} \tag{18}$$

$$\Delta P = \frac{KLQ^n(2n+1)^n}{2^{n+1}\,\text{arccosh}\left(\frac{H_{\max}}{H_{\min}}\right) W^n n^{n+1} H_{\min}^{2n+1}} \text{Im}\left[{}_2F_1\left(\frac{1}{2}, -n; 1-n; \frac{H_{\max}^2}{H_{\min}^2}\right)\right], \quad \text{for hyperbolic cosine} \tag{19}$$

and

$$\Delta P = \frac{KLQ^n(2n+1)^n}{2^{n+1}\pi W^n n^{n+1} H_{\max}^{2n}\sqrt{H_{\max}H_{\min}}} \text{Im}\left(F_1\left(-2n; \frac{1}{2}, \frac{1}{2}; 1-2n; 1, \frac{H_{\max}}{H_{\min}}\right)\right), \quad \text{for the sinusoidal,} \tag{20}$$

converging-diverging channels respectively, where ${}_2F_1$ is the hypergeometric function, $\text{Im}\,({}_2F_1)$ is the imaginary part of the hypergeometric function and F_1 is the imaginary part of the Appell hypergeometric function in equations (17)-(20). It is worth mentioning that all these relationships maintain dimensional consistency and validated for a Newtonian fluid flow.

3 Flow resistance for branching network

We define the maximum to minimum radius ratio and channel-height ratio for the network tubes and channels at the k-th generation as

$$\frac{R_{\max,k+1}}{R_{\min,k+1}} = \frac{R_{\max,k}}{R_{\min,k}} = e_t, \qquad \text{and} \qquad \frac{H_{\max,k+1}}{H_{\min,k+1}} = \frac{H_{\max,k}}{H_{\min,k}} = e_c, \tag{21}$$

respectively. Using the $\Delta P - Q$ relation for the various converging-diverging tubes and rectangular channels from the previous section, from equations (8), (13) to (16) along with equation (21), we can easily write $\Delta P - Q$ relation for the converging-diverging tubes at the k-th generation as

$$\Delta P_k = \phi_i \frac{L_k Q_k^n}{R_{\min,k}^{3n+1}}, \tag{22}$$

and from equations (12), (17) to (20) along with equation (21), we can easily write $\Delta P - Q$ relation for the converging-diverging channels at the k-th generation as

$$\Delta P_k = \xi_i \frac{L_k Q_k^n}{W_k^n H_{\min,k}^{2n+1}}, \tag{23}$$

where for the linear, parabolic, hyperbolic, hyperbolic cosine and sinusoidal converging-diverging tubes, by comparing the equations the ϕ_i and ξ_i are independent of the varying geometrical parameters

between the generations level k and depends upon the fluid properties n, K, or the maximum-minimum radius/height ratio e_t and e_c, respectively. Also, the L_k is the length of the tube, and R_k is the radius of the tube, where the $R_{\max,k}$ and $R_{\min,k}$ denote the radius at the most divergent and convergent part of the tube at the k-th generation. For the channels, the W_k is the constant width in a branch at the k-th generation, the H_k represents the varying cross–sectional mid-height across length with $H_{\max,k}$ and $H_{\min,k}$ denote the channel-height at the most divergent and convergent part of the upper-part/lower-part of the channel at the k-th generation. Also ΔP_k and Q_k are the respective pressure drop and the flow rate at the k_{th} level branch. Therefore, by defining the flow resistance $\mathcal{R}_k$ for the tube and the channel in a k_{th} level branch, we can write

$$\mathcal{R}_k = \frac{\Delta P_k}{Q_k^n} = \phi_i \frac{L_k}{R_{\min,k}^{3n+1}} \qquad \text{for the tube,} \tag{24}$$

and

$$\mathcal{R}_k = \frac{\Delta P_k}{Q_k^n} = \xi_i \frac{L_k}{W_k^n H_{\min,k}^{2n+1}} \qquad \text{for the channel,} \tag{25}$$

respectively. For each branching generation k, the radius and length for the tube can be scaled by factors β and γ, such as $\beta = \dfrac{R_k}{R_{k-1}} = \dfrac{R_{\max,k}}{R_{\max,k-1}} = \dfrac{R_{\min,k}}{R_{\min,k-1}}$, and $\gamma = \dfrac{L_k}{L_{k-1}}$, respectively. Thus, for the k-th generation, we have

$$R_k = R_0\beta^k,\ R_{\max,k} = R_{\max,0}\beta^k,\ R_{\min,k} = R_{\min,0}\beta^k \qquad \text{and} \qquad L_k = L_0\gamma^k, \tag{26}$$

respectively. Similarly for each branching generation k in the channel networks, the height, width and length for the channels can be scaled by factors β, α and γ, such as $\beta = \dfrac{H_k}{H_{k-1}} = \dfrac{H_{\max,k}}{H_{\max,k-1}} = \dfrac{H_{\min,k}}{H_{\min,k-1}}$, $\alpha = \dfrac{W_k}{W_{k-1}}$, and $\gamma = \dfrac{L_k}{L_{k-1}}$, respectively. Thus, for the k-th generation, we have

$$H_k = H_0\beta^k,\ H_{\max,k} = H_{\max,0}\beta^k,\ H_{\min,k} = H_{\min,0}\beta^k,\ W_k = W_0\alpha^k \qquad \text{and} \qquad L_k = L_0\gamma^k, \tag{27}$$

respectively. Substituting the defined scaling into the resistance formula, we obtain

$$\mathcal{R}_k = \frac{\Delta P_k}{Q_k^n} = \phi_i \frac{L_0}{R_{\min,0}^{3n+1}} \left(\frac{\gamma}{\beta^{(3n+1)}}\right)^k, \tag{28}$$

for the tube and

$$\mathcal{R}_k = \frac{\Delta P_k}{Q_k^n} = \xi_i \frac{L_0}{W_0^n H_{\min,0}^{2n+1}} \left(\frac{\gamma}{\alpha^n \beta^{(2n+1)}}\right)^k, \tag{29}$$

for the channel network, respectively. Further, we define the total network resistance $\mathcal{R}_t$ as

$$\mathcal{R}_t = \frac{\Delta P}{Q^n}, \tag{30}$$

where

$$\Delta P = \sum_{k=0}^{m} \Delta P_k. \tag{31}$$

Here, the total pressure drop across the network is denoted by ΔP, and Q represents the total flow rate within the network. Here, $k = 0$ and m signify the first and last generations, respectively. Within the network, at each generation, branches split into N new ones. Consequently, at the k-th generation, there are N^k branches. Additionally, the flow rate Q_k through each branch equals the total flow rate Q divided by the number of branches N^k. Therefore, considering equations (28) through (31), the total resistance for the tube network and channel network leads to

$$\mathcal{R}_t = \frac{\Delta P}{Q^n} = \frac{1}{Q^n}\sum_{k=0}^{m}\Delta P_k = \sum_{k=0}^{m}\frac{\mathcal{R}_k Q_k^n}{Q^n} = \sum_{k=0}^{m}\frac{\mathcal{R}_k}{(N^n)^k} = \phi_i \frac{L_o}{R_{\min,0}^{3n+1}}\sum_{k=0}^{m}\left(\frac{\gamma}{N^n\ \beta^{(3n+1)}}\right)^k, \tag{32}$$

and

$$\mathcal{R}_t = \frac{\Delta P}{Q^n} = \frac{1}{Q^n}\sum_{k=0}^{m}\Delta P_k = \sum_{k=0}^{m}\frac{\mathcal{R}_k Q_k^n}{Q^n} = \sum_{k=0}^{m}\frac{\mathcal{R}_k}{(N^n)^k} = \xi_i \frac{L_0}{W_0^n H_{\min,0}^{2n+1}}\sum_{k=0}^{m}\left(\frac{\gamma}{N^n\ \alpha^n\ \beta^{(2n+1)}}\right)^k, \tag{33}$$

respectively. Substituting this into equations (32), (74) as well as utilizing geometric series summation, we obtain the total resistance for the tube network and channel network as

$$\mathcal{R}_t = \phi_i \frac{L_o}{R_{\min,o}^{3n+1}}\left(\left[1-\left(\frac{\gamma}{N^n\ \beta^{(3n+1)}}\right)^{m+1}\right]\Bigg/\left[1-\frac{\gamma}{N^n\ \beta^{(3n+1)}}\right]\right), \tag{34}$$

and

$$\mathcal{R}_t = \xi_i \frac{L_o}{W_o^n H_{\min,o}^{2n+1}}\left(\left[1-\left(\frac{\gamma}{N^n\ \alpha^n\ \beta^{(2n+1)}}\right)^{m+1}\right]\Bigg/\left[1-\frac{\gamma}{N^n\ \alpha^n\ \beta^{(2n+1)}}\right]\right), \tag{35}$$

respectively.

3.1 Flow conductance E for self-similar tube networks under volume and surface area constraint

The total volume and surface area of the k_{th} level branch in a linear converging-diverging tube is given by

$$V_k = 2\pi\int_0^{L_k/2}(a+bx)_k^2 dx = \frac{\pi(e_t^2+e_t+1)}{3}L_k R_{\min,k}^2, \tag{36}$$

and

$$S_k = 4\pi\int_0^{L_k/2}(a+bx)_k dx = \pi(e_t+1)L_k R_{\min,k}, \tag{37}$$

respectively. Therefore upon summation over the whole network, the total volume and surface area of the network considering the number of branches N yields

$$V = \frac{\pi(e_t^2+e_t+1)}{3}R_{\min,0}^2 L_0\sum_{k=0}^{m}\left(N\beta^2\gamma\right)^k \qquad \text{and} \qquad S = \pi(e_t+1)R_{\min,0}L_0\sum_{k=0}^{m}\left(N\beta\gamma\right)^k, \tag{38}$$

respectively. This is a geometric series with the common ratio $N\beta^2\gamma$ and $N\beta\gamma$ for volume and surface-area, respectively. Summing the series, we get

$$V = \psi_{i,v} R_{\min,0}^2 L_0 \frac{1-(N\beta^2\gamma)^{m+1}}{1-N\beta^2\gamma} \qquad \text{and} \qquad S = \Psi_{i,s} R_{\min,0} L_0 \frac{1-(N\beta\gamma)^{m+1}}{1-N\beta\gamma}, \tag{39}$$

where for the linear converging-diverging tube, the $\psi_{i,v}(e_t) = \dfrac{\pi(e_t^2+e_t+1)}{3}$, and the $\Psi_{i,s}(e_t) = \pi(e_t+1)$. Similarly the volume and surface area of the tube for other converging-diverging sections such as parabolic, hyperbolic, hyperbolic cosine and sinusoidal can be evaluated as (39), where $\psi_{i,v}(e_t)$, and the $\Psi_{i,s}(e_t)$ which have different values but are dependent only on the constant ratio $R_{\max,k}/R_{\min,k} = e_t$. Also, the total length of the network is

$$L = L_0 \frac{1-\gamma^{m+1}}{1-\gamma} \tag{40}$$

Further, using the total volume and surface area constraint with the same length as of network in a single equivalent tube, we get the equivalent radius under these two volume and surface area constraint for all converging-diverging tube network sections as

$$R_{\min,s}|_V = R_{\min,0}\left(\frac{1-\gamma}{1-\gamma^{m+1}}\frac{1-(N\beta^2\gamma)^{m+1}}{1-N\beta^2\gamma}\right)^{1/2}, \text{ and } R_{\min,s}|_S = R_{\min,0}\left(\frac{1-\gamma}{1-\gamma^{m+1}}\frac{1-(N\beta\gamma)^{m+1}}{1-N\beta\gamma}\right), \tag{41}$$

respectively. Using equation (41), flow resistance under volume and surface area constraint of single equivalent tube for all converging-diverging tube network yields

$$\mathcal{R}_s|_V = \phi_i \frac{L_s}{R_{\min,s}^{3n+1}} = \phi_i \frac{L_0}{R_{\min,0}^{3n+1}} \left[\frac{1-\gamma^{m+1}}{1-\gamma}\right]^{(3n+3)/2} \left[\frac{1-N\beta^2\gamma}{1-(N\beta^2\gamma)^{m+1}}\right]^{(3n+1)/2}, \tag{42}$$

and

$$\mathcal{R}_s|_S = \phi_i \frac{L_s}{R_{\min,s}^{3n+1}} = \phi_i \frac{L_0}{R_{\min,0}^{3n+1}} \left[\frac{1-\gamma^{m+1}}{1-\gamma}\right]^{(3n+2)} \left[\frac{1-N\beta\gamma}{1-(N\beta\gamma)^{m+1}}\right]^{(3n+1)}, \tag{43}$$

respectively. Further, the non-dimensional flow conductance E of the network, defined as the ratio of total flow conductance $E_t = 1/\mathcal{R}_t$ to the equivalent single tube flow conductance $E_s = 1/\mathcal{R}_s$ under volume and surface area constraint for all converging-diverging tube network leads to

$$E|_{V,\text{tube}} = \frac{1/\mathcal{R}_t}{1/\mathcal{R}_s} = \frac{\mathcal{R}_s}{\mathcal{R}_t} = \left[\frac{1-\gamma^{m+1}}{1-\gamma}\right]^{(3n+3)/2} \left[\frac{1-N\beta^2\gamma}{1-(N\beta^2\gamma)^{m+1}}\right]^{(3n+1)/2} \left[\frac{1-\gamma/N^n\beta^{(3n+1)}}{1-(\gamma/N^n\beta^{(3n+1)})^{m+1}}\right], \tag{44}$$

and

$$E|_{S,\text{tube}} = \frac{\mathcal{R}_s}{\mathcal{R}_t} = \left[\frac{1-\gamma^{m+1}}{1-\gamma}\right]^{(3n+2)} \left[\frac{1-N\beta\gamma}{1-(N\beta\gamma)^{m+1}}\right]^{(3n+1)} \left[\frac{1-\gamma/N^n\beta^{(3n+1)}}{1-(\gamma/N^n\beta^{(3n+1)})^{m+1}}\right], \tag{45}$$

respectively.

3.2 Flow conductance E for self-similar rectangular channel networks under volume and surface area constraint

Similar formulation for the flow conductance can be derived for the self-similar rectangular channel networks. The total volume and surface area of the k_{th} level branch in a linear converging-diverging rectangular channel is given by

$$V_k = 4W_k \int_0^{L_k/2} (a+bx)_k dx = (e_c+1)W_k L_k H_{\min,k}, \tag{46}$$

and

$$S_k = 4\int_0^{L_k/2} (W_k + 2(a+bx)_k)dx = 4\pi \int_0^{L_k/2} (a+bx)_k dx = 2L_k(W_k + (e_c+1)H_{\min,k}), \tag{47}$$

respectively. Therefore upon summation over the whole network, the total volume and surface area of the network considering the number of branches N yields

$$V = (e_c+1)H_{\min,0}L_0W_0\sum_{k=0}^{m}(N\alpha\beta\gamma)^k, \text{ and } S = 2W_0L_0\sum_{k=0}^{m}(N\alpha\gamma)^k + 2(e_c+1)H_{\min,0}L_0\sum_{k=0}^{m}(N\beta\gamma)^k, \tag{48}$$

respectively. This is a geometric series with the common ratio $N\alpha\beta\gamma$ for volume; and $N\alpha\gamma$, $N\beta\gamma$ for the surface-area, respectively. Summing the series, we get

$$V = \psi_{i,v}H_{\min,0}L_0W_0\frac{1-(N\alpha\beta\gamma)^{m+1}}{1-N\alpha\beta\gamma}, \text{ and } S = \Psi_{i,s,1}W_0L_0\frac{1-(N\alpha\gamma)^{m+1}}{1-N\alpha\gamma} + \Psi_{i,s,2}H_{\min,0}L_0\frac{1-(N\beta\gamma)^{m+1}}{1-N\beta\gamma}, \tag{49}$$

respectively, where for the linear converging-diverging rectangular channel, the $\psi_{i,v}(e_c) = (e_c+1)$, $\Psi_{i,s,1} = 2$, and the $\Psi_{i,s,2} = 2(e_c+1)$. Similarly the volume and surface area of the tube for other converging-diverging sections such as parabolic, hyperbolic, hyperbolic cosine and sinusoidal can be evaluated as (49), where $\psi_{i,v}(e_c)$, $\Psi_{i,s,1}(e_c)$, and $\Psi_{i,s,2}(e_c)$ which have different values but are dependent only on the constant ratio $H_{\max,k}/H_{\min,k} = e_c$. Further, using the total volume constraint with the same length and width as of network in a single equivalent rectangular channel, we get the equivalent height and width under volume constraint for all converging-diverging rectangular channel network sections as

$$W_s|_V = W_0\frac{1-\alpha^{m+1}}{1-\alpha}, \text{ and } H_{\min,s}|_V = H_{\min,0}\left(\frac{1-\gamma}{1-\gamma^{m+1}}\frac{1-\alpha}{1-\alpha^{m+1}}\frac{1-(N\alpha\beta\gamma)^{m+1}}{1-N\alpha\beta\gamma}\right), \tag{50}$$

Similarly, the single equivalent rectangular channel surface area can be defined as

$$S_s = \Psi_{i,s,1}W_sL_s + \Psi_{i,s,2}H_{\min,s}L_s. \tag{51}$$

By comparing equation (49) and (51), we get the equivalent width and height under the total surface area constraint with the same length as of the network in a single equivalent rectangular channel for all converging-diverging rectangular channel network sections as

$$W_s|_S = W_0\left(\frac{1-\gamma}{1-\gamma^{m+1}}\frac{1-(N\alpha\gamma)^{m+1}}{1-N\alpha\gamma}\right), \text{ and } H_{\min,s}|_S = H_{\min,0}\left(\frac{1-\gamma}{1-\gamma^{m+1}}\frac{1-(N\beta\gamma)^{m+1}}{1-N\beta\gamma}\right), \tag{52}$$

respectively. Using equation (50), and (52) with (25), the flow resistance under volume and surface area constraint of single equivalent tube for all converging-diverging tube network yields

$$\mathcal{R}_s|_V = \xi_i \frac{L_s}{W_s^n H_{\min,s}^{2n+1}} = \xi_i \frac{L_0}{W_0^n H_{\min,0}^{2n+1}} \left[\frac{1-\gamma^{m+1}}{1-\gamma}\right]^{(2n+2)} \left[\frac{1-\alpha^{m+1}}{1-\alpha}\right]^{(n+1)} \left[\frac{1-N\alpha\beta\gamma}{1-(N\alpha\beta\gamma)^{m+1}}\right]^{(2n+1)}, \tag{53}$$

and

$$\mathcal{R}_s|_S = \xi_i \frac{L_s}{W_s^n H_{\min,s}^{2n+1}} = \xi_i \frac{L_0}{W_0^n H_{\min,0}^{2n+1}} \left[\frac{1-\gamma^{m+1}}{1-\gamma}\right]^{(3n+2)} \left[\frac{1-N\alpha\gamma}{1-(N\alpha\gamma)^{m+1}}\right]^{n} \left[\frac{1-N\beta\gamma}{1-(N\beta\gamma)^{m+1}}\right]^{(2n+1)}, \tag{54}$$

respectively. Further, the non-dimensional flow conductance E of the network, defined as the ratio of total flow conductance $E_t = 1/\mathcal{R}_t$ to the equivalent single tube flow conductance $E_s = 1/\mathcal{R}_s$ under volume and surface area constraint for all converging-diverging rectangular channel network leads to

$$\begin{aligned} E|_{V,\text{channel}} &= \frac{1/\mathcal{R}_t}{1/\mathcal{R}_s} = \frac{\mathcal{R}_s}{\mathcal{R}_t} \\ &= \left[\frac{1-\gamma^{m+1}}{1-\gamma}\right]^{(2n+2)} \left[\frac{1-\alpha^{m+1}}{1-\alpha}\right]^{(n+1)} \left[\frac{1-N\alpha\beta\gamma}{1-(N\alpha\beta\gamma)^{m+1}}\right]^{(2n+1)} \left[\frac{1-\gamma/N^n\alpha^n\beta^{(2n+1)}}{1-(\gamma/N^n\alpha^n\beta^{(2n+1)})^{m+1}}\right], \end{aligned} \tag{55}$$

and

$$\begin{aligned} E|_{S,\text{channel}} &= \frac{1/\mathcal{R}_t}{1/\mathcal{R}_s} = \frac{\mathcal{R}_s}{\mathcal{R}_t} \\ &= \left[\frac{1-\gamma^{m+1}}{1-\gamma}\right]^{(3n+2)} \left[\frac{1-N\alpha\gamma}{1-(N\alpha\gamma)^{m+1}}\right]^{n} \left[\frac{1-N\beta\gamma}{1-(N\beta\gamma)^{m+1}}\right]^{(2n+1)} \left[\frac{1-\gamma/N^n\alpha^n\beta^{(2n+1)}}{1-(\gamma/N^n\alpha^n\beta^{(2n+1)})^{m+1}}\right], \end{aligned} \tag{56}$$

respectively.

4 Results and Discussion

Building upon the comprehensive analysis of flow conductance for the power-law shear-thinning and thickening fluid flow by preserving the volume and the surface area of the converging-diverging tubes and rectangular channels networks (refer sections 3.1 and 3.2), we can delve deeper into the influence of network geometry on optimal design for a given fluid flow. Equations (44) and (45) highlight the critical role of geometrical parameters (m, N, γ, and β) in converging-diverging tubes fractal branching networks. Further, equations (55) and (56) highlight the critical role of geometrical parameters (m, α , N, γ, and β) in converging-diverging rectangular channels fractal branching networks. Using these equations, we can establish the relationship between effective flow conductance ratio E and the network's geometrical characteristics. This paves the way for uncovering the scaling laws governing the optimal radius and height ratio for the power-law shear-thinning and thickening fluid flow in the converging-diverging tubes and rectangular channels, respectively.

4.1 Volume constrained networks for converging-diverging tubes

We find that the non-dimensional flow conductance E of the linear, parabolic, hyperbolic, hyperbolic cosine and sinusoidal converging-diverging tubes network under volume and surface area constraint leads to the same flow conductance E as derived by Garg et al. [1] for the power-law fluids in circular tubes. Hence the results and scaling for all converging-diverging tubes networks remains the same. These scaling are that the maximum flow conductance occurs when a dimensionless radius ratio β^* satisfies the equation $\beta^* = N^{-1/3}$, and $\beta^* = N^{-(n+1)/(3n+2)}$ under constrained tube-volume and surface-area, respectively. Here, N represents the bifurcation number of branches splitting at each junction and n is the fluid power-law index. Further, the optimal condition occur at the equipartition of pressure drop across each branching level. Therefore in the next section we directly show the new results on the converging diverging rectangular channels in detail.

4.2 Volume constrained networks for converging diverging rectangular channels

4.2.1 Effect of γ, α, m, and N

Figure 3(a)-(l) shows E for the power-law fluid flow in the linear, parabolic, hyperbolic, hyperbolic cosine and sinusoidal converging-diverging tree-like rectangular channels network under the constraint volume, plotted against the β for varying combinations of channel-length ratios γ (a-c), at $N = 4$, $\alpha = 0.35$, and $m = 3$; for various combinations of branching levels m (d-f) at $\gamma = 0.6$, $\alpha = 0.35$, and $N = 4$; for varying combinations of channel-width ratio α (g-i) at $m = 3$, $N = 5$ and $\gamma = 0.6$ and for varying combinations of branching splitting numbers N (j-l) at $m = 3$, $\alpha = 0.35$ and $\gamma = 0.6$. The figures (a,d,g,j) show results for $n = 0.5$, (b,e,h,k) for $n = 1$ and (c,f,i,l) for $n = 1.5$, respectively. We observe a non-linear correlation between β and E in all figures. This suggests that, E is influenced by all parameters γ, α, m, and N. Initially E increases with β and reaches a peak and subsequently declines. This maximum E corresponds to an optimal β^* defined in equation (55).

For $\beta \approx 0$, E tends towards zero, regardless of n, γ, α, m, and N, reflecting the minimal conductance. This zero flow conductance remains for larger β values as power-law index n increases. Furthermore, the steepness of E increases with increase in n. Moreover, the maximum E at the optimal ratio β^* decreases for all power-law indices n as γ, α, m, and N increase.

In all figures 3(a)-(l), the optimal β^* remains identical regardless of γ and m, for all n. However, β^* varies with both α with values like $\beta^* = 0.5,\ 0.58,\ 0.71, 1$ for $\alpha = 0.2,\ 0.4,\ 0.6,\ 0.8$, respectively, as well as with N such as $\beta^* = 0.69,\ 0.76,\ 0.85, 0.98$ for $N = 3,\ 4,\ 5,\ 6$, respectively . Moreover, at a given value of α and N, the β^* remains the same for all n. Furthermore, as the channel-width α as well as the branching N increases, both the β^* and corresponding E decreases.

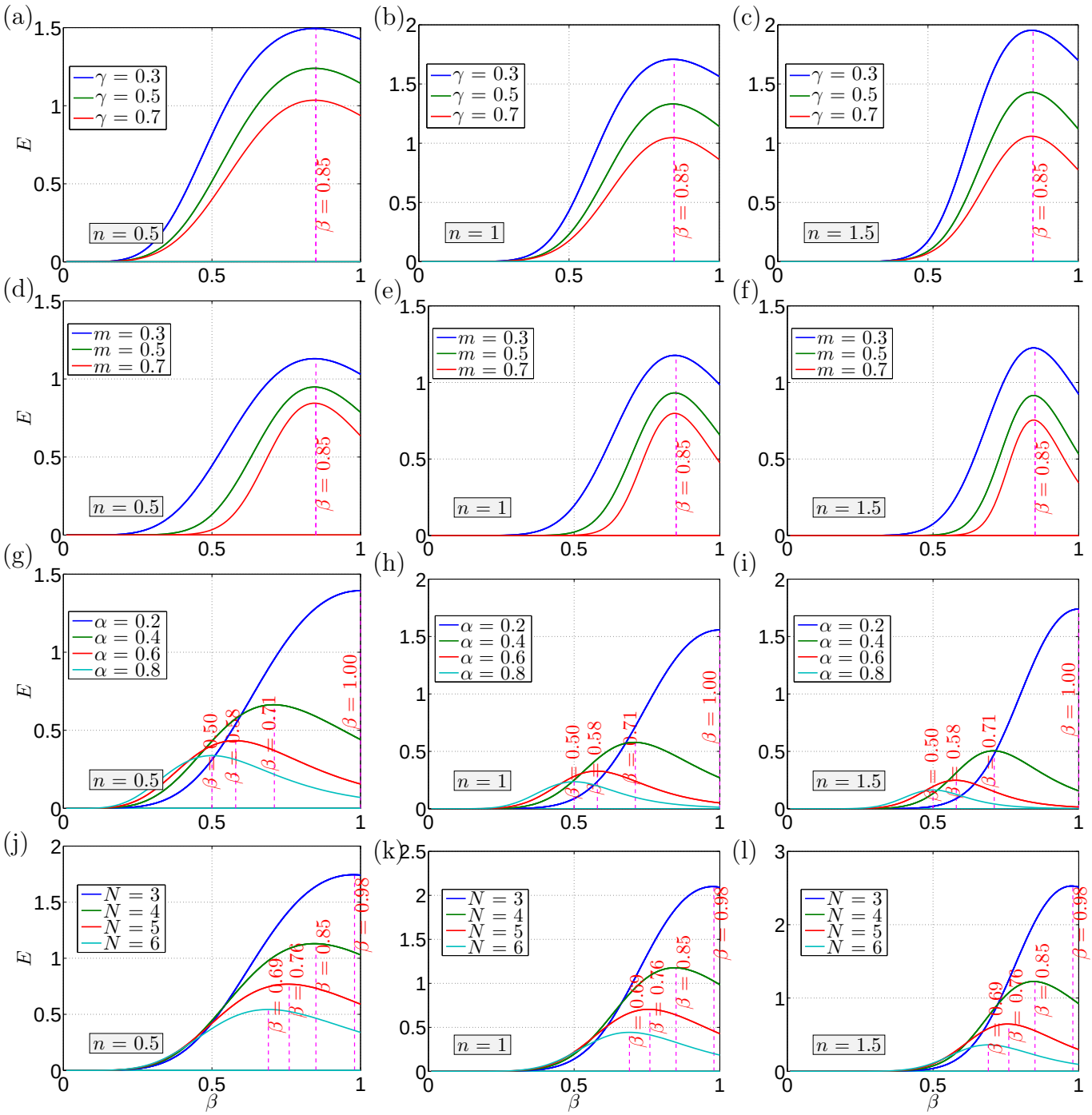

Figure 3: The flow-conductance E of the power-law fluid flow in the linear, parabolic, hyperbolic, hyperbolic cosine and sinusoidal converging-diverging tree-like rectangular channels network under the volume constraint, plotted against the β for varying combinations of channel-length ratios γ (a-c), at $N = 4$, $\alpha = 0.35$, and $m = 3$; for various combinations of branching levels m (d-f) at $\gamma = 0.6$, $\alpha = 0.35$, and $N = 4$; for varying combinations of channel-width α (g-i) at $m = 3$, $N = 5$ and $\gamma = 0.6$ and for varying combinations of branching splitting numbers N (j-l) at $m = 3$, $\alpha = 0.35$ and $\gamma = 0.6$. The figures (a,d,g,j) show results for $n = 0.5$, (b,e,h,k) for $n = 1$ and (c,f,i,l) for $n = 1.5$, respectively.

4.2.2 Optimal parameters and scaling law

Figure 4(a) and 4(b) shows that the optima β^* for maximum E varies with the N at given α and vice versa, respectively. We show the plot on log-log scale. Our findings reveal a power-law relationship among the optimal height ratio β^*, the channel-width ratio α and the number of branching rectangular channels N in the network. This relationship can be expressed as: $\beta^* \propto \alpha^{s_1}\ N^{s_2}$, where s_1, and s_1 are the scaling exponent.

In order to understand that how β^* scales with the channel-width α and the branching N, we can minimise the total resistance of one parent-child network at k^{th} branching level as

$$\mathcal{R}_t = \sum_{k=k}^{k+1} \frac{\mathcal{R}_k}{(N^n)^k} = \xi_i \left(\frac{L_k}{(N^n)^k\ W_k^n\ H_{\min,k}^{(2n+1)}} + \frac{L_{k+1}}{(N^n)^{k+1}\ W_{k+1}^n\ H_{\min,k+1}^{(2n+1)}} \right). \tag{57}$$

There exist a minimum resistance and optimal solution for given length and the channel width, such that $\dfrac{d\mathcal{R}_t}{dH_{\min,k}} = 0$. Similar to Garg et al. [1], minimising equation (57) is equivalent to minimise,

$$\mathcal{M} = \frac{L_k}{(N^n)^k\ W_k^n\ H_{\min,k}^{(2n+1)}} + \frac{L_{k+1}}{(N^n)^{k+1}\ W_{k+1}^n\ H_{\min,k+1}^{(2n+1)}}, \tag{58}$$

under the volume constraint of

$$V = \psi_{i,v}(N)^k H_{\min,k} L_k W_k + \psi_{i,v}(N)^{k+1}\ H_{\min,k+1} L_{k+1} W_{k+1}. \tag{59}$$

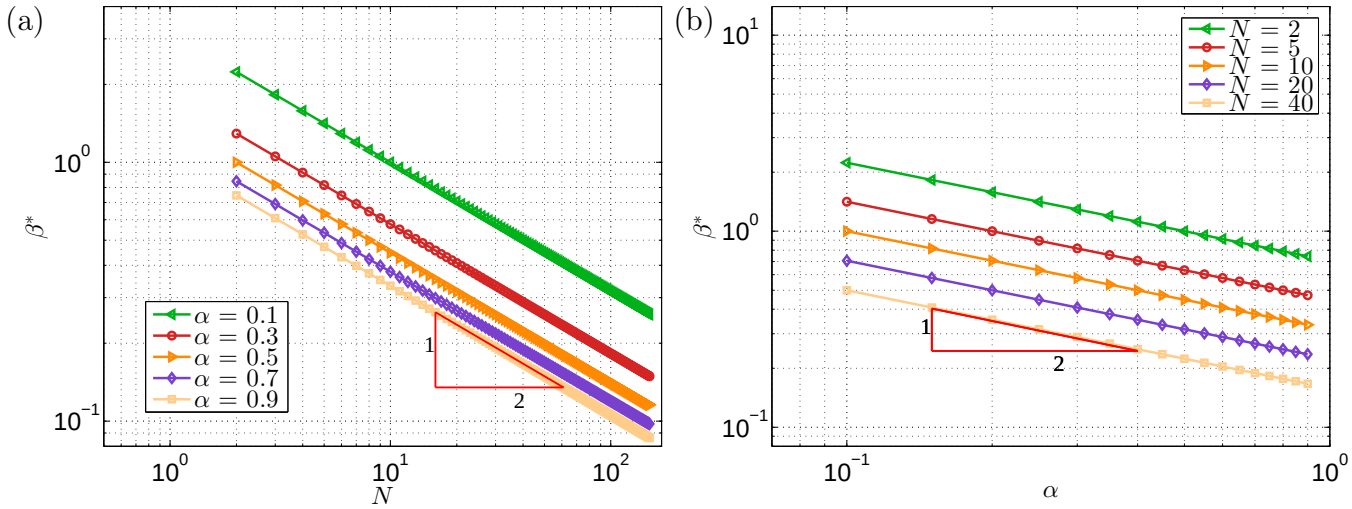

Figure 4: Figure (a) and (b) shows that the optimal β^* for maximum E varies with the N at given α and vice versa, respectively. We show the plot on log-log scale. Our findings reveal a power-law relationship among the optimal height ratio β^*, the channel-width ratio α and the number of branching rectangular channels N in the network. This relationship can be expressed as: $\beta^* \propto \alpha^{s_1}\ N^{s_2}$, where s_1, and s_1 are the scaling exponent. This is true for all fluid index n for all linear, parabolic, hyperbolic, hyperbolic cosine and sinusoidal converging-diverging tree-like rectangular channels network under volume constraint.

Assuming

$$x = H_{\min,k}, \qquad \text{and} \qquad y = H_{\min,k+1}, \tag{60}$$

we get

$$\mathcal{M} = \frac{L_k}{(N^n)^k\ W_k^n\ x^{(2n+1)}} + \frac{L_{k+1}}{(N^n)^{k+1}\ W_{k+1}^n\ (A - Bx)^{(2n+1)}}, \tag{61}$$

where $A = V/(\psi_{i,v}(N)^{k+1} L_{k+1} W_{k+1})$ and $B = L_k W_k/(N\ L_{k+1} W_{k+1})$. Further, differentiating with x, we get

$$\frac{d\mathcal{M}}{dx} = 0 \implies \frac{-L_k}{(N^n)^k\ W_k^n\ x^{(2n+2)}} + \frac{BL_{k+1}}{(N^n)^{k+1}\ W_{k+1}^n\ (A - Bx)^{(2n+2)}} = 0. \tag{62}$$

which further implies

$$\left(\frac{(A - Bx)}{x}\right)^{(2n+2)} = \left(\frac{H_{\min,k+1}}{H_{\min,k}}\right)^{(2n+2)} = N^{-(n+1)}\alpha^{-(n+1)}. \tag{63}$$

$$\frac{H_{\min,k+1}}{H_{\min,k}} = \beta^* = N^{-1/2}\alpha^{-1/2}. \tag{64}$$

As β^* at any k^{th} level is independent of k. Therefore, this scaling hold true in complete linear, parabolic, hyperbolic, hyperbolic cosine and sinusoidal converging-diverging tree-like rectangular channels network. Further, optimal height ratio β^* is also independent of the length ratio γ, m and power-law index n of the power-law fluids. Further, by comparing the relationship $\beta^* \propto \alpha^{s_1}\ N^{s_2}$, we get $s_1 = -1/2$ and $s_2 = -1/2$ for all n. Also, using equation (64), we get

$$\left(\frac{Q_{k+1}}{Q_k}\right)^* = \frac{1}{N} = \left(\frac{H_{\min,k+1}}{H_{\min,k}}\right)^2 \left(\frac{W_{k+1}}{W_k}\right) \implies Q_k \propto H_{\min,k}^2 W_k, \qquad \text{for all } n. \tag{65}$$

Under a limiting case for the rectangular channel with $\beta = 1$, we get the $\alpha^* = N^{-1}$, which has been derived by Jing and Zhan [34] and validate our more genelise formulation for varying height and width of five converging-diverging tree-like rectangular channels geometries.

4.3 Surface-area constrained networks for converging diverging rectangular channels

4.3.1 Effect of γ, α, m, and N

Figure 5(a)-(l) shows E for the power-law fluid flow in the linear, parabolic, hyperbolic, hyperbolic cosine and sinusoidal converging-diverging tree-like rectangular channels network under the constraint surface area, plotted against the β for varying combinations of channel-length ratios γ (a-c), at $N = 4$, $\alpha = 0.35$, and $m = 3$; for various combinations of branching levels m (d-f) at $\gamma = 0.6$, $\alpha = 0.35$, and $N = 4$; for varying combinations of channel-width ratio α (g-i) at $m = 3$, $N = 5$ and $\gamma = 0.6$ and for varying combinations of branching splitting numbers N (j-l) at $m = 3$, $\alpha = 0.35$ and $\gamma = 0.6$. The figures (a,d,g,j) show results for $n = 0.5$, (b,e,h,k) for $n = 1$ and (c,f,i,l) for $n = 1.5$, respectively. We observe a non-linear correlation between β and E in all figures. This suggests that, E is influenced

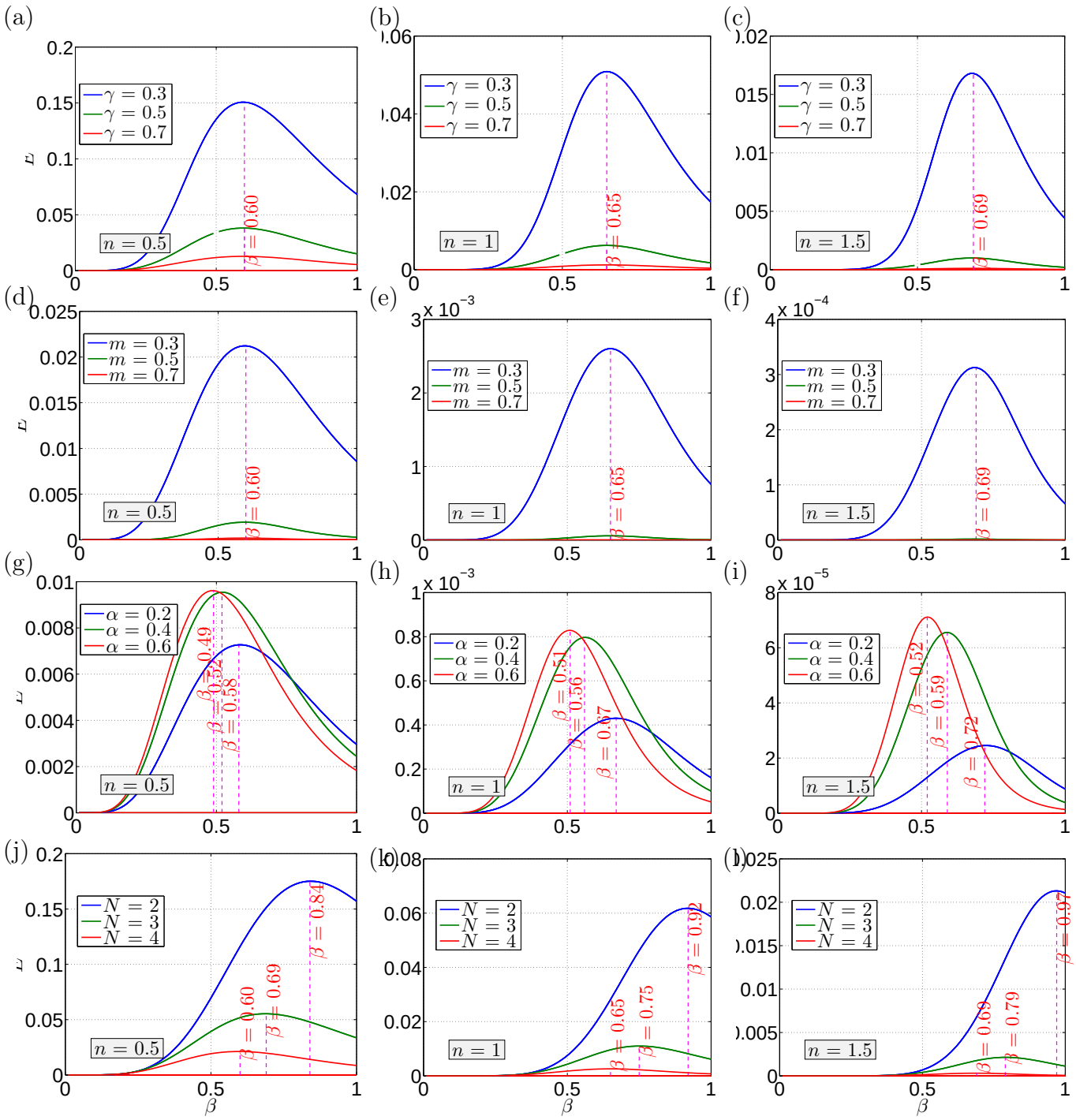

Figure 5: The flow-conductance E of the power-law fluid flow in the linear, parabolic, hyperbolic, hyperbolic cosine and sinusoidal converging-diverging tree-like rectangular channels network under the surface-area constraint, plotted against the β for varying combinations of channel-length ratios γ (a-c), at $N = 4$, $\alpha = 0.35$, and $m = 3$; for various combinations of branching levels m (d-f) at $\gamma = 0.6$, $\alpha = 0.35$, and $N = 4$; for varying combinations of channel-width α (g-i) at $m = 3$, $N = 5$ and $\gamma = 0.6$ and for varying combinations of branching splitting numbers N (j-l) at $m = 3$, $\alpha = 0.35$ and $\gamma = 0.6$. The figures (a,d,g,j) show results for $n = 0.5$, (b,e,h,k) for $n = 1$ and (c,f,i,l) for $n = 1.5$, respectively.

by all parameters γ, α, m, and N. Initially E increases with β and reaches a peak and subsequently declines. This maximum E corresponds to an optimal β^* defined in equation (56).

For $\beta \approx 0$, E tends towards zero, regardless of n, γ, α, m, and N, reflecting the minimal conductance. This zero flow conductance remains for larger β values as power-law index n increases. Furthermore, the steepness of E increases with increase in n. Moreover, the maximum E at the optimal ratio β^* decreases for all power-law indices n as γ, α, m, and N increase.

In all figures 5(a)-(l), the optimal β^* remains identical regardless of γ and m, for a given n. However, it depends on fluid index n, where as n, increases, β^* also increases. Further, β^* varies with α with values like $\beta^* = 0.49,\ 0.52,\ 0.58$, $\beta^* = 0.51,\ 0.56,\ 0.67$ and $\beta^* = 0.52,\ 0.59,\ 0.72$ at $\alpha = 0.2,\ 0.4,\ 0.6$ for $n = 0.5$, $n = 1$, and $n = 1.5$ respectively. Furthermore, β^* also varies with N with values like $\beta^* = 0.6,\ 0.69,\ 0.84$, $\beta^* = 0.65,\ 0.75,\ 0.92$, $\beta^* = 0.69,\ 0.79,\ 0.97$ at $N = 2,\ 3,\ 4$, for $n = 0.5$, $n = 1$, and $n = 1.5$ respectively. Moreover, at a given value of α and N, the β^* increase as n increases. Furthermore, as the channel-width α as well as the branching N increases, both the β^* and corresponding E decreases.

4.3.2 Optimal parameters and scaling law

Figure 6(a-c) and 7(a-c) shows that the optimal β^* for maximum E varies with the N at given α and vice versa, respectively for a given n. We show the plot on log-log scale. Our findings reveal a power-law relationship among the optimal height ratio β^*, the channel-width ratio α and the number of branching rectangular channels N in the network. This relationship can be expressed as: $\beta^* \propto \alpha^{s_3}\ N^{s_4}$, where s_3, and s_4 are the scaling exponent.

In order to understand that how β^* scales with the channel-width α and the branching N, we can minimise the total resistance of one parent-child network at k^{th} branching level as

$$\mathcal{R}_t = \sum_{k=k}^{k+1} \frac{\mathcal{R}_k}{(N^n)^k} = \xi_i \left(\frac{L_k}{(N^n)^k\ W_k^n\ H_{\min,k}^{(2n+1)}} + \frac{L_{k+1}}{(N^n)^{k+1}\ W_{k+1}^n\ H_{\min,k+1}^{(2n+1)}} \right). \tag{66}$$

There exist a minimum resistance and optimal solution for given length and the channel width, such that $\dfrac{d\mathcal{R}_t}{dH_{\min,k}} = 0$. Similar to Garg et al. [1], minimising equation (66) is equivalent to minimise,

$$\mathcal{M}_s = \frac{L_k}{(N^n)^k\ W_k^n\ H_{\min,k}^{(2n+1)}} + \frac{L_{k+1}}{(N^n)^{k+1}\ W_{k+1}^n\ H_{\min,k+1}^{(2n+1)}}, \tag{67}$$

under the surface area constraint of

$$S = \Psi_{i,s,1} N^k W_k L_k + \Psi_{i,s,2} (N^n)^k H_{\min,k} L_k + \Psi_{i,s,1} N^{k+1} W_{k+1} L_{k+1} + \Psi_{i,s,2} (N^n)^{k+1} H_{\min,k+1} L_{k+1}. \tag{68}$$

Assuming

$$x = H_{\min,k}, \qquad \text{and} \qquad y = H_{\min,k+1}, \tag{69}$$

we get

$$\mathcal{M}_s = \frac{L_k}{(N^n)^k\ W_k^n\ x^{(2n+1)}} + \frac{L_{k+1}}{(N^n)^{k+1}\ W_{k+1}^n\ (A_s - B_s x)^{(2n+1)}}, \tag{70}$$

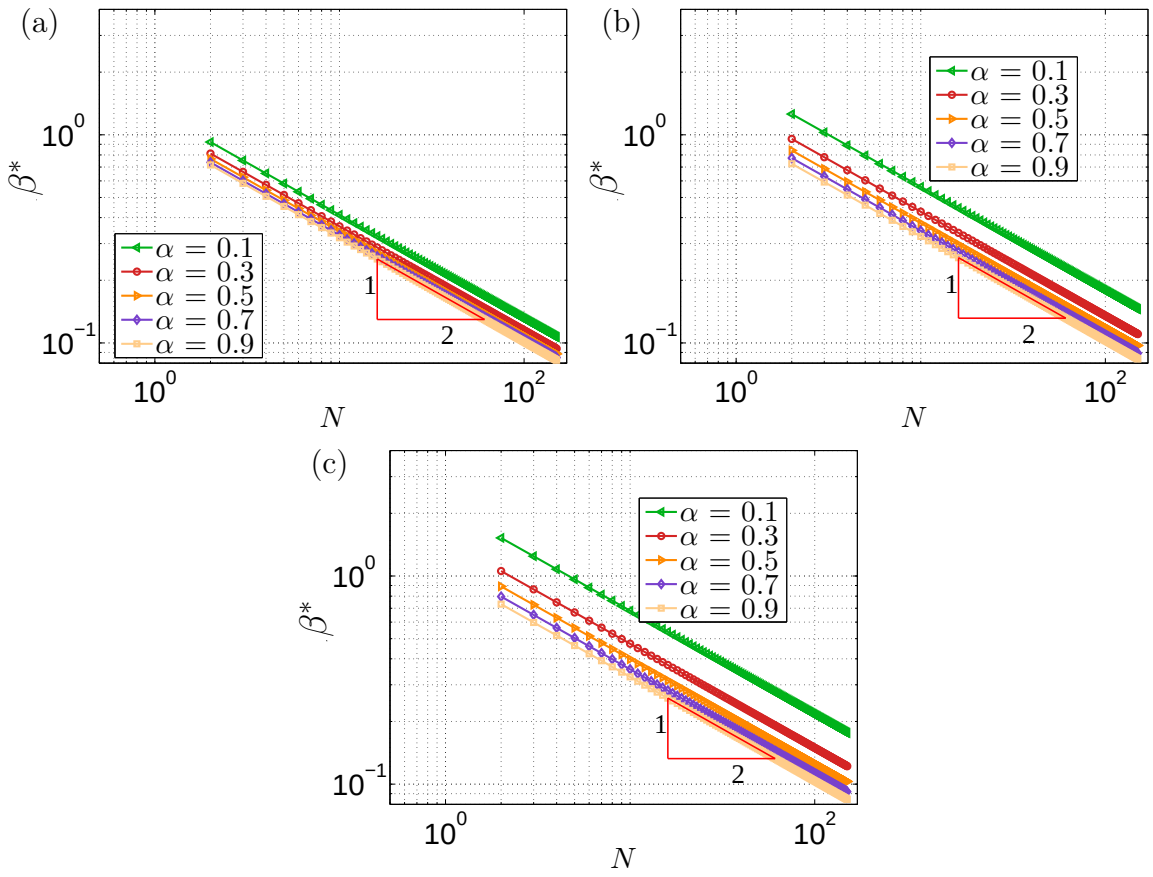

Figure 6: We show the optimal β^* for maximum E varies with the N at given α for (a) $n = 0.5$, (b) $n = 1$, and (c) $n = 1.5$, respectively for all linear, parabolic, hyperbolic, hyperbolic cosine and sinusoidal converging-diverging tree-like rectangular channels network under surface-area constraint. The plot is on the log-log scale.

where

$$A_s = \frac{S - \Psi_{i,s,1} N^k W_k L_k - \Psi_{i,s,1} N^{k+1} W_{k+1} L_{k+1}}{\Psi_{i,s,2} N^{k+1} L_{k+1}} \tag{71}$$

and

$$B_s = \frac{L_k}{N\ L_{k+1}}, \tag{72}$$

respectively. Further, differentiating with x, we get

$$\frac{d\mathcal{M}_s}{dx} = 0 \implies \frac{-L_k}{(N^n)^k\ W_k^n\ x^{(2n+2)}} + \frac{BL_{k+1}}{(N^n)^{k+1}\ W_{k+1}^n\ (A_s - B_s x)^{(2n+2)}} = 0. \tag{73}$$

which further implies

$$\left(\frac{(A_s - B_s x)}{x}\right)^{(2n+2)} = \left(\frac{H_{\min,k+1}}{H_{\min,k}}\right)^{(2n+2)} = N^{-(n+1)} \alpha^{-n}. \tag{74}$$

$$\frac{H_{\min,k+1}}{H_{\min,k}} = \beta^* = N^{-1/2} \alpha^{-n/(2n+2)}. \tag{75}$$

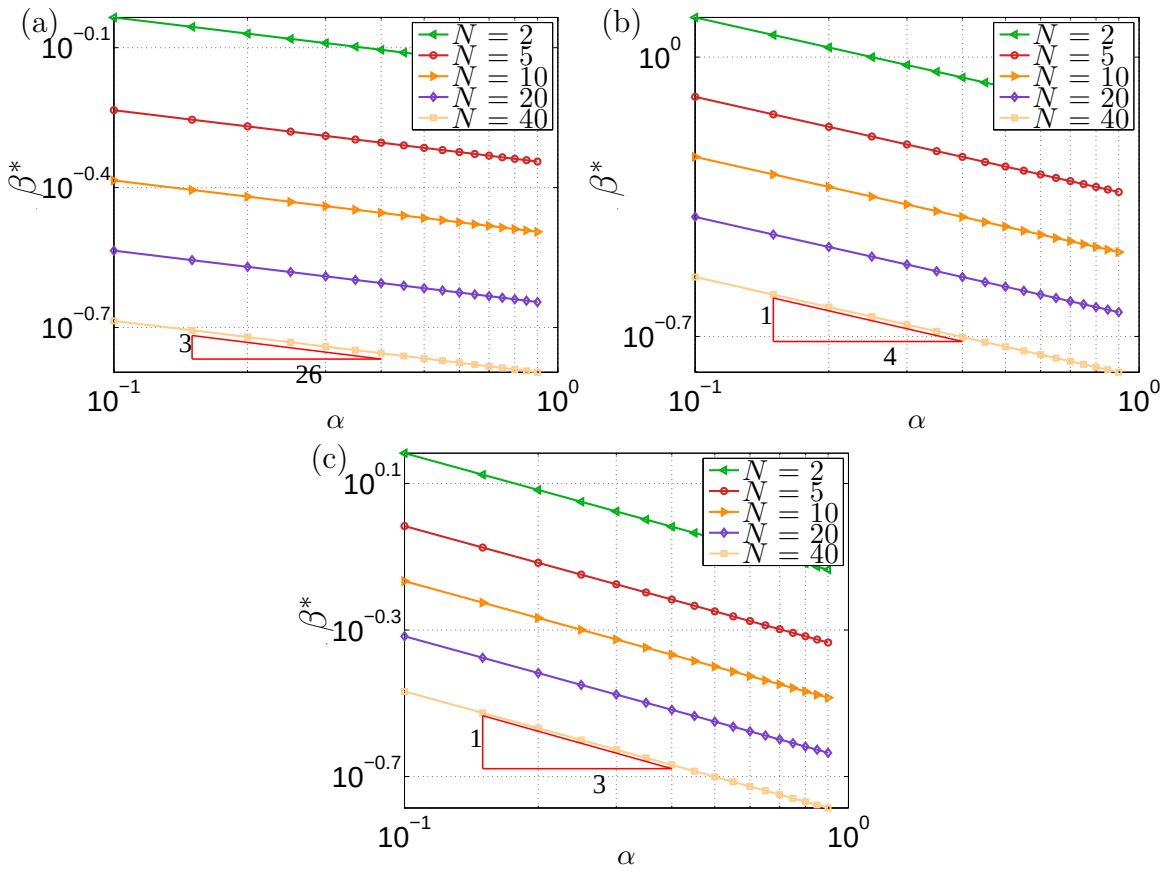

Figure 7: We show the optimal β^* for maximum E varies with the α at given N for (a) $n = 0.5$, (b) $n = 1$, and (c) $n = 1.5$, respectively for all linear, parabolic, hyperbolic, hyperbolic cosine and sinusoidal converging-diverging tree-like rectangular channels network under surface-area constraint. The plot is on the log-log scale.

As β^* at any k^{th} level is independent of k. Therefore, this scaling hold true in complete linear, parabolic, hyperbolic, hyperbolic cosine and sinusoidal converging-diverging tree-like rectangular channels network. Further, optimal height ratio β^* is also independent of the length ratio γ, and m at a given power-law index n of the power-law fluids. Further, by comparing the relationship $\beta^* \propto \alpha^{s_3}\ N^{s_4}$, we get $s_3 = -1/2$ and $s_4 = -n/(2n+2)$ for all n. Also, using equation (75), we get

$$\left(\frac{Q_{k+1}}{Q_k}\right)^* = \frac{1}{N} = \left(\frac{H_{\min,k+1}}{H_{\min,k}}\right)^2 \left(\frac{W_{k+1}}{W_k}\right)^{n/(n+1)} \implies Q_k \propto H_{\min,k}^2 W_k^{n/(n+1)}, \quad \text{for all } n. \tag{76}$$

The analysis focuses on the optimal height ratio for minimum flow resistance or maximum flow conductance E. By analyzing how the optimal β^* scales with channel-width ratio α, and the number of branches N, we gain insights into how the network design needs to adapt for efficient flow with varying branching complexities. The β^* is not constant but changes with the channel-width ratio α and number of daughter branches N with scaling exponent -1/2 each in case of constraint volume of the channels and $-n/(2n+2)$ and $-1/2$ in case of constraint surface-area of the channels. This highlights the influence of the channel-width ratio and the bifurcation number on the optimal design

in the linear, parabolic, hyperbolic, hyperbolic cosine and sinusoidal converging-diverging tree-like rectangular channels networks. This type of analysis helps in designing efficient branching networks for fluid flow in various applications.

5 Conclusions

This study generalizes Murray's Law by incorporating a non-Newtonian power-law fluid model within various converging-diverging dendritic networks of tubes and rectangular channels with arbitrary bifurcation number N and generation level m. We analyzed five different converging-diverging profiles as linear, parabolic, hyperbolic, hyperbolic cosine and sinusoidal converging-diverging dendritic network. We introduce two constraints: constant total tube volume (relevant for natural flow) and constant total surface area (important for industrial and heat/mass transfer applications) assuming steady, incompressible, 2D planar and axisymmetric laminar flow without considering network losses in this study. Analyzing networks with arbitrary N, m, power-law index n, and channel width ratio α allows for a broader applicability.

We define a dimensionless effective flow conductance E to quantify flow behavior based on the parent-daughter radius or channel height ratio β, length ratio γ, N, α and m. Our results show that dimensionless effective flow conductance decreases with increasing length ratio, N, α and m. The peak conductance is reached when a specific radius/channel-height ratio, denoted as β, is attained, contingent upon both the constraints and the vessel's geometry, whether it be tubular or rectangular in shape. Interestingly, this ratio remains consistent regardless of the type of converging-diverging profile along the vessel's length. Our investigation confirms that this scaling, indicated by $\beta^*_{\max} = \beta^*_{\min} = N^{-1/3}$ for tube volume constraints and $\beta^*_{\max} = \beta^*_{\min} = N^{-(n+1)/(3n+2)}$ for surface area constraints, aligns with the findings of Garg et al. [1] regarding power-law fluid flow in uniform tubes. In this context, $\beta_{\max}$ and $\beta_{\min}$ represent the radius ratios between parent and daughter branches at the most divergent or convergent parts of the vessel, respectively. Here, N denotes the number of branches dividing at each junction, and n signifies the power-law index of the fluid. Importantly, under the volume and surface-constraint constraint for the Newtonian fluids in the converging-diverging tubes, the classic Murray's Law scaling remains valid at the optimal condition.

Furthermore, we found that the optimal flow scaling for height ratio in rectangular channels is $\beta^*_{\max} = \beta^*_{\min} = N^{-1/2}\alpha^{-1/2}$ for tube volume constraints and $\beta^*_{\max} = \beta^*_{\min} = N^{-1/2}\alpha^{-n/(2n+2)}$ for surface area constraints in all converging-diverging channel networks, where α is the channel-width ratio between parent and daughter branches. Under a limiting case for the rectangular channel with $\beta = 1$, we get the $\alpha^* = N^{-1}$, which has been derived by Jing and Zhan [34] and validate our scaling law which are more generalise formulation for varying height and width of five converging-diverging tree-like rectangular channels geometries. Our findings are substantiated through experimentation, comparison with existing theories under limiting conditions as shown by Garg et al. [1] for the uniform tube-networks, and an expansion of Hess-Murray's law to encompass shear-thinning and shear-thickening fluids across varying branching numbers N.

In conclusion, this work expands Murray's Law by incorporating non-Newtonian power-law fluid behavior under both volume and surface area constraints in the various converging-diverging dendritic networks of tubes and rectangular channels. The findings reveal different optimal scaling and design principles depending on the constraint, cross-sectional geometry of the vessel and fluid properties such as n for optimizing flow in tree-like branching networks.

Data availability statement

All data generated and analyzed during this study are included within this manuscript.

References

[1] Ashish Garg, Himanshu Mishra, and Sudip K Pattanayek. Scaling laws for optimised power-law fluid flow in self-similar tree-like branching networks. *ChemRxiv- Chemical Engineering and Industrial Chemistry, DOI: 10.26434/chemrxiv-2024-cj754*, pages 1–30, 2024.

[2] Benoit B Mandelbrot and Benoit B Mandelbrot. *The fractal geometry of nature*, volume 1. WH Freeman New York, 1982.

[3] Marc-Olivier Coppens. Nature-inspired chemical engineering for process intensification. *Annual Review of Chemical and Biomolecular Engineering*, 12:187–215, 2021.

[4] Ross J Metzger, Ophir D Klein, Gail R Martin, and Mark A Krasnow. The branching programme of mouse lung development. *Nature*, 453(7196):745–750, 2008.

[5] Adrian Bejan. *Shape and structure, from engineering to nature*. Cambridge university press, 2000.

[6] Alireza Yazdani, R Appiah Otoo, and Paul Jeffrey. Resilience enhancing expansion strategies for water distribution systems: A network theory approach. *Environmental Modelling & Software*, 26(12):1574–1582, 2011.

[7] David Rhys Morgan and Ian C Goulter. Optimal urban water distribution design. *Water resources research*, 21(5):642–652, 1985.

[8] Ashish Garg, Nico Bergemann, Beccy Smith, Matthias Heil, and Anne Juel. Fluidisation of yield stress fluids under vibration. *Journal of Non-Newtonian Fluid Mechanics*, 294:104595, 2021.

[9] Ashish Garg. Fluidisation of yield stress materials under vibration. *PhD thesis, The University of Manchester*, pages 1–175, 2022.

[10] Petru Niga, Jonas Örtegren, Viviane Alecrim, Marianne Klaman, Erik Blohm, and Jon Lofthus. Hybrid printing: paper media for combined flexographic and inkjet printing. In *2012 International Paper Physics Conference, Stockholm, June 10-14, 2012*, pages 79–81. Innventia, 2012.

[11] Johanna Johnson. *Aspects of flexographic print quality and relationship to some printing parameters*. PhD thesis, Karlstad University, 2008.

[12] Richard Coles and Mark J Kirwan. *Food and beverage packaging technology*. John Wiley & Sons, 2011.

[13] F Bozzoli, L Cattani, and S Rainieri. Cross-helix corrugation: The optimal geometry for effective food thermal processing. *International Journal of Heat and Mass Transfer*, 147:118874, 2020.

[14] John Vlachopoulos and Nickolas D Polychronopoulos. Understanding rheology and technology of polymer extrusion, 2019.

[15] A Lewandowski and K Wilczyński. Global modeling of single screw extrusion with slip effects. *International Polymer Processing*, 34(1):81–90, 2019.

[16] Beatriz R Oliveira, Rodrigo FO Borges, P Leônidas Filho, Pedro R Villares, Eduardo CH Paraíso, Bruno F Oechsler, José MS Rocha, LuísA Calçada, and Cláudia M Scheid. Modeling and simulation of non-newtonian fluid flows and heat transfer in a non-isothermal coiled tubing to oil well operations. *Geoenergy Science and Engineering*, page 211980, 2023.

[17] Sreedevi Lingadahalli Kotreshappa, Chempi Gurudas Nayak, and Santhosh Krishnan Venkata. A review on the role of microflow parameter measurements for microfluidics applications. *Systems*, 11(3):113, 2023.

[18] Qiuxian Luo, Rongjie Xu, Keke Wang, Jian He, Changjun Liu, Pan Wu, and Wei Jiang. Continuous separation of oil/water mixture by a double-layer corrugated channel structure with superhydrophobicity and superoleophilicity. *Separation and Purification Technology*, 269:118647, 2021.

[19] Reza Izadi and Ali Moosavi. Electrowetting of power-law fluids in microgrooved channels. *Physics of Fluids*, 32(7), 2020.

[20] Santtu TT Ollila, Colin Denniston, Mikko Karttunen, and Tapio Ala-Nissila. Biopolymer filtration in corrugated nanochannels. *Physical review letters*, 112(11):118301, 2014.

[21] Ashish Garg. Enhanced flow in deformable carbon nanotubes. *Journal of Applied Physics*, 135 (7), 2024.

[22] M Khoshvaght-Aliabadi, A Feizabadi, and SF Khaligh. Empirical and numerical assessments on corrugated and twisted channels as two enhanced geometries. *International journal of mechanical sciences*, 157:25–44, 2019.

[23] Garima Vishal, Ashish Garg, Jayati Sarkar, and Sudip K Pattanayek. The channel flow of a real shear thickening fluid using the lattice boltzmann simulation and the theoretical model. *ChemRxiv- Chemical Engineering and Industrial Chemistry, DOI: 10.26434/chemrxiv-2023-zk1nn*, pages 1–26, 2023.

[24] Garima Vishal, Ashish Garg, Jayati Sarkar, and Sudip Kumar Pattanayek. Real shear thickening fluid (stf) flow in converging-diverging channels: Analytical and lattice boltzmann study. *ChemRxiv- Chemical Engineering and Industrial Chemistry, DOI: 10.26434/chemrxiv-2023-3cjvq*, pages 1–29, 2023.

[25] Cecil D Murray. The physiological principle of minimum work: I. the vascular system and the cost of blood volume. *Proceedings of the National Academy of Sciences*, 12(3):207–214, 1926.

[26] Rémi Revellin, François Rousset, David Baud, and Jocelyn Bonjour. Extension of murray's law using a non-newtonian model of blood flow. *Theoretical Biology and Medical Modelling*, 6:1–9, 2009.

[27] Ashish Garg, Himanshu Mishra, and Sudip K. Pattanayek. Optimal flow and scaling laws for power-law fluids in elliptical cross-section self-similar tree-like networks. *ChemRxiv- Chemical Engineering and Industrial Chemistry, DOI: 10.26434/chemrxiv-2024-lc1sz*, pages 1–22, 2024.

[28] Ashish Garg, Himanshu Mishra, Jayati Sarkar, and Sudip K Pattanayek. Scaling laws for optimal turbulent flow in tree-like networks with smooth and rough tubes and power-law fluids. *ChemRxiv- Chemical Engineering and Industrial Chemistry, DOI: 10.26434/chemrxiv-2024-2zt43*, pages 1–20, 2024.

[29] Ashish Garg. Scaling laws for optimal herschel–bulkley yield stress fluid flow in self-similar tree-like branching networks. *ChemRxiv- Chemical Engineering and Industrial Chemistry, DOI: 10.26434/chemrxiv-2024-f0hg7*, 2024.

[30] Jing J Lee, Jean Berthier, Kathleen E Kearney, Erwin Berthier, and Ashleigh B Theberge. Open-channel capillary trees and capillary pumping. *Langmuir*, 36(43):12795–12803, 2020.

[31] Ashish Garg. Pulsatile pressure enhanced rapid water transport through flexible graphene nano/angstrom-size channels: a continuum modeling approach using the micro-structure of nanoconfined water. *New Journal of Physics*, 25(10), 2023.

[32] Ashish Garg and Swati Bishnoi. An empirical experimental observations and md simulation data-based model for the material properties of confined fluids in nano/angstrom size tubes. *Nano Express*, 5(1), 2023. doi: 10.1088/2632-959X/ad2b83.

[33] Himanshu Mishra and Ashish Garg. Heuristic modeling of material properties in nano/angstrom-scale channels: Integrating experimental observations and md simulations. *ChemRxiv-Nanoscience, DOI: 10.26434/chemrxiv-2024-57w1p*, pages 1–19, 2024.

[34] Dalei Jing and Xuekuan Zhan. Cross-sectional dimension dependence of electroosmotic flow in fractal treelike rectangular microchannel network. *Micromachines*, 11(3):266, 2020.

[35] Biliang Tu, Boqi Xiao, Yidan Zhang, and Gongbo Long. An analytical model for permeability of fractal tree-like branched networks composed of converging–diverging capillaries. *Physics of Fluids*, 36(4), 2024.

[36] Taha Sochi. The flow of power-law fluids in axisymmetric corrugated tubes. *Journal of Petroleum Science and Engineering*, 78(3-4):582–585, 2011.

[37] Ashish Garg. Power-law fluid flow in diverse converging-diverging geometries of corrugated channels. *ChemRxiv- Chemical Engineering and Industrial Chemistry, DOI: 10.26434/chemrxiv-2024-5ssd9*, pages 1–15, 2024.

[38] R Byron Bird, Robert C Armstrong, and Ole Hassager. Dynamics of polymeric liquids. vol. 1: Fluid mechanics. 1987.